Communications in Physics, Vol. 35, No. 4 (2025), pp. 403-415
DOI: https://doi.org/10.15625/0868-3166/22744

Numerical study of thermal lensing and focal shift in 1064 nm fiber laser cutting heads 1-6 kW

Do Thanh Tung[1,2]

[1]*Academy of Military Science and Technology, Nghia Do, Hanoi, Vietnam*
[2]*ITMO University, 197101 Saint Petersburg, Russia*

E-mail: †tungitmo@gmail.com

Received 3 April 2025
Accepted for publication 11 September 2025
Published 9 December 2025

Abstract. *Thermal lensing is an inherent phenomenon in high-power laser optical systems, including fiber laser cutting heads, arising from energy absorption–induced thermal and optical variations. This paper presents a numerical study, based on the finite element method, of thermal lensing effects in a 1064 nm fiber laser system operating at 1–6 kW, using fused silica plano-convex lenses with focal lengths of 125–300 mm. The simulations predict a maximum lens temperature of 952 K at 6 kW, leading to focal shifts up to* $\Delta f = -45.4$ *mm for a 300 mm focusing lens, and relative refractive index variations of 74.5–114%. While spot diagram asymmetries appear at higher power levels, these are likely numerical artifacts rather than physical optical deformation. The results highlight the significant impact of thermal lensing on focal stability and provide a numerical framework useful for the design and optimization of fiber laser cutting heads operating at kilowatt power levels.*

Keywords: thermal lensing; fiber laser; finite element method; focus shift.
Classification numbers: 02.70.Dh; 42.60.-v; 44.05.+e.

1. Introduction

Fiber laser cutting heads (1–6 kW, 1064 nm) are vital for precision machining, industrial component fabrication, and high-precision parts in aerospace, medical, and electronics industries. They also support specialized applications, including nuclear facility dismantling, underwater cutting, robotic operations, and rock fragmentation in tunnel boring machines [1–6]. The ability to transmit laser beams via optical fibers allows remote placement of the laser source, simplifying equipment needs, while the non-contact nature of laser cutting enhances flexibility and precision when integrated with robotic arms [7].

However, thermal lensing, an inherent challenge in high-power laser systems, degrades performance [8–12]. Energy absorption by optical components and anti-reflective coatings creates temperature gradients, altering the lens's refractive index and inducing phase distortions. This results in focal shifts and, in simpler cases, a thermal lens effect that displaces the focal point [13–16]. Uncontrolled focal shifts reduce machining accuracy, particularly in thick metal processing, where high power density and precise beam focus are critical for optimal cutting speed and edge quality. Thermal effects also increase the beam propagation factor (M^2), causing higher-order aberrations that impair beam quality [10]. Although optical cooling mitigates overall temperature, local gradients persist, making thermal lensing unavoidable [12].

Understanding refractive index variations due to thermal effects is crucial for predicting focal shifts and optimizing laser cutting. Controlling optical distortions improves beam quality, stabilizes power density, enhances accuracy, and reduces material waste, thereby lowering costs. While prior studies explored focal shifts with different materials and coatings [13–16], systems with varying focal lengths remain underexplored. This study uses numerical simulations to investigate focal shift variations in a high-power (1–6 kW) fiber laser cutting head, quantifying refractive index changes across focusing lenses with focal lengths of 125–300 mm. It also analyzes beam spreading and distortions at the focal plane, with the aim of assessing the applicability and limitations of the finite element method for simulating thermo-optical effects in high-power fiber laser systems.

2. Methodology, modeling and theory

2.1. Laser cutting head simulation

The fiber laser cutting head, operating at 1–6 kW and 1064 nm, typically uses continuous-wave mode but supports pulsed operation. As shown in Figure 1, the laser beam from a fiber input is collimated by a collimating lens, then focused by a focusing lens with an adjustable mechanism ($+15/-25$ mm range for a 100 mm collimator / 200 mm focusing lens) to optimize the focal point on the material surface [17–19]. A protection window shields internal optics from dust, spatter, and back-reflections. An assist gas system (oxygen, nitrogen, or argon, ≤ 30 bar) delivers gas through a nozzle to remove molten material and enhance cut quality. Water or air cooling stabilizes the temperature of optical components, minimizing thermal deformation. Some systems integrate water spray cooling with assist gas to reduce workpiece back-reflections, ensuring stable, high-precision operation for industrial metal processing.

Optical lenses are critical for shaping and focusing beams in high-power laser cutting heads. Commonly used materials include fused silica and N-BK7 [13, 16], with alternatives like N-PSK53, N-PPK51, and CaF_2 also employed [14]. Fused silica, with a low thermal expansion coefficient ($\sim 0.55 \times 10^{-6}\,K^{-1}$) [13] and minimal absorption at 1064 nm, ensures thermal stability and low energy loss, ideal for high-power applications [13, 16]. Anti-reflective (AR) coatings, including uncoated, wavelength-specific, and broadband types, enhance efficiency at 1064 nm, achieving reflectance reductions exceeding 99% [20, 21], with some reaching 99.99% [22]. The optical system comprises two plano-convex fused silica lenses (50 mm diameter, 3 mm edge thickness): a collimating lens (100 mm focal length) and a focusing lens (125, 150, 200, or 300 mm focal length). Focusing lenses, nearer the cutting zone, require frequent replacement due to thermal lensing and coating degradation.

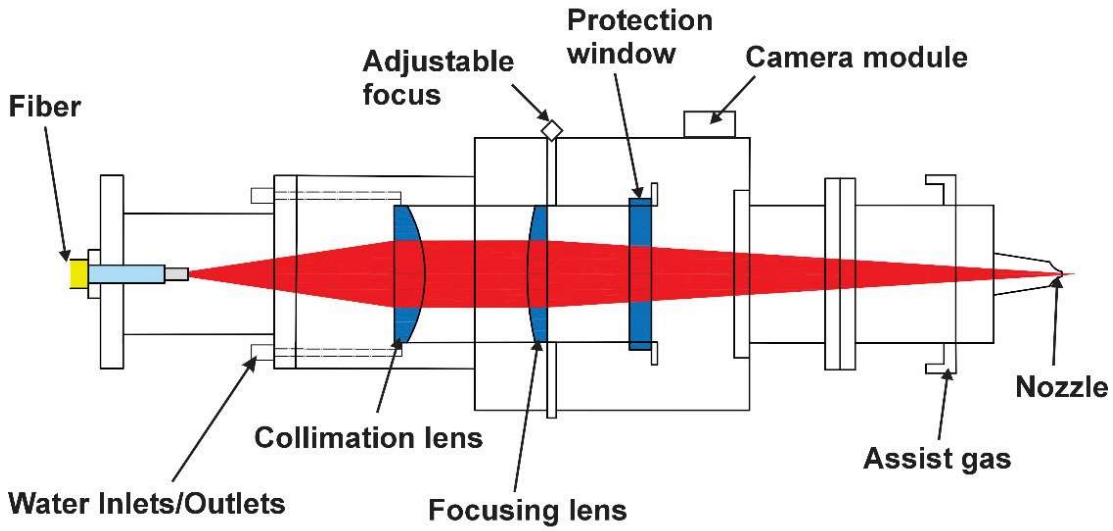

Fig. 1. Internal scheme of the laser cutting head.

In practical high-power laser cutting systems, active cooling mechanisms such as water-cooled or air-cooled assemblies are typically employed to mitigate thermal effects in optical components [1, 2]. However, in this study, active cooling was not employed in order to evaluate the maximum impact of thermal lensing under natural convection conditions. The obtained results provide valuable insights into how thermal lensing depends on focal length and laser power, and serve as a useful reference for evaluating the necessity and effectiveness of active cooling in future system designs.

This study uses finite element method (FEM) simulations in COMSOL Multiphysics 6.1. A 1 W baseline assumes negligible thermal effects. The simulation couples Geometrical Optics, Heat Transfer in Solids, and Solid Mechanics to model ray trajectories, temperature, and thermal expansion. At the fiber output, the laser beam has a wavelength of 1064 nm, a numerical aperture (NA) of 0.1, and follows a Gaussian intensity profile normalized at the $1/e^2$ level. The beam diameter at the fiber output is set to 200 μm, which is consistent with high-power fiber laser cutting systems (1–6 kW) typically employing large-core fibers [17, 19]. An AR coating (99.5% transmittance at 1064 nm) is applied to the lens surface to minimize reflection losses of the Gaussian beam. At the focal plane, a 1 mm circular planar annulus is used to capture the deposited power for power distribution analysis. Lenses are fixed with an 80 mm separation. Optical parameters of collimating and focusing lenses are listed in Table 1.

The Geometrical Optics interface traces ray paths using a Hamiltonian-based ray tracing method, releasing 9000 rays in a conical hexapolar distribution (18 rings) to represent the beam profile. Ray power attenuates according to:

$$P = P_0 \exp[-2k_0 \kappa L], \tag{1}$$

where k_0 is the free-space wave number, L is the optical path length, and n and κ represent the real and imaginary parts of the refractive index of the medium or material, respectively; P_0 denotes the

Table 1. Optical parameters of collimating and focusing lenses.

	1	**2**	**3**	**4**	**5**
Radius of curvature, R_1 [mm]	∞	56.8	68.8	90.8	135.8
Radius of curvature, R_2 [mm]	45.8	∞	∞	∞	∞
Center thickness, d [mm]	10.425	8.7976	7.7029	6.5095	5.321
Focal length [mm]	≈ 100	≈ 125	≈ 150	≈ 200	≈ 300

average laser power. This equation applies to weakly absorbing media, with the condition $\kappa \ll n$, which holds for fused silica at 1064 nm. Positive values of κ correspond to an attenuating medium, while negative values indicate a wave-amplifying medium.

Absorbed laser power is modeled as a volumetric heat source in the *Heat Transfer in Solids* interface, solving the heat equation with convective boundary conditions (heat transfer coefficient 10 W/m^2·K [23, 24], ambient temperature 293 K). A Bidirectionally Coupled Ray Tracing study, with three iterations, ensures self-consistent ray trajectories and lens deformation. The FEM model uses cubic Lagrange shape functions for temperature and displacement to minimize numerical error. The computational mesh employs free tetrahedral elements (maximum size 3 mm), refined to 0.5 mm at fixed boundaries and 0.025 mm at the target plane for accurate focal spot analysis.

2.2. Theoretical analysis of thermal lensing effects

To calculate the temperature distribution within the lens, we employ a numerical model based on FEM. The heat conduction equation in a solid medium is expressed as:

$$\rho c_p \frac{\partial T}{\partial t} = \nabla \cdot (k \nabla T) + Q, \tag{2}$$

where ρ [kg/m^3], c_p, and k represent the density, specific heat capacity, and thermal conductivity of fused silica, respectively; Q denotes the heat source term due to laser energy absorption.

The volumetric heat source $Q(r,z)$ is caused by laser energy absorption within the lens. This follows Beer–Lambert's law:

$$Q(r,z) = Q_0(r)\, e^{-\kappa z}, \tag{3}$$

where $Q(r,z)$ [W/m^3] is the heat source density, representing the energy absorbed per unit volume by the laser beam within the lens, with κ [m^{-1}] as the optical absorption coefficient and z [m] as the wave propagation depth. This emphasizes the per-unit dependence (per unit area and length), preventing misinterpretation as the total absorbed energy.

The temperature-dependent refractive index change in the lens can be expressed using a linear relationship:

$$n(T) = n_0 + \frac{dn}{dT}(T - T_0), \tag{4}$$

where $n(T)$ and n_0 represent the refractive index of the material at temperature T and reference temperature T_0, respectively. $\frac{dn}{dT}$ is the thermo-optic coefficient. It is assumed that the nonlinear variation of $\frac{dn}{dT}$ with temperature is negligible [25, 26]. As temperature T increases, the resulting refractive index change alters the effective focal length of the focusing lens, leading to a focal plane shift. The linear relationship between the focal shift (Δf) and the temperature gradient for a

lens can be expressed as [10]:

$$\Delta f = A\,\frac{P_0}{D_b}, \tag{5}$$

where A is the absorptivity of the lens, D_b is the diameter of the incident beam, and P_0 is the average input power of the laser beam.

The lens surface exchanges heat with the surrounding environment through natural convection in this study. The boundary condition is described by Newton's law of convective heat transfer:

$$q_{\text{conv}} = h(T - T_{\text{ambient}}), \tag{6}$$

where q_{conv} [W/m^2] is the heat flux density exchanged through the lens surface, h is the convective heat transfer coefficient of air, and T_{ambient} [K] is the ambient air temperature.

In the optical system of a high-power laser cutting head, spot size governs power density and cutting quality. The root mean square (RMS) spot size, a key metric for beam focusing, is calculated as:

$$r_{\text{RMS}} = \sqrt{\frac{1}{N}\sum_{i=1}^{N}(r_i - r_0)^2}, \tag{7}$$

where r_{RMS} is the RMS beam radius, N is the number of rays, r_i is the distance of the i-th ray from the optical axis at the focal plane, and r_0 is the distance of the beam center from the optical axis at the focal plane. A smaller r_{RMS} value indicates better beam focusing at the focal plane. In cases where the laser beam exhibits axial symmetry, the initial beam radius can be approximated as $r_0 \approx 0$.

Assuming a Gaussian beam distribution for the incident laser beam, we have:

$$I(r) = I_0 \exp\left(-\frac{2r^2}{\omega^2}\right), \tag{8}$$

where the intensity I_0 is related to the average beam power P_0 for a Gaussian beam through the relationship

$$P_0 = \frac{1}{2}\pi\omega^2 I_0,$$

and ω is the beam radius at the $1/e^2$ intensity point.

The absorbed power density at a given point within the lens is calculated as:

$$Q(r,z) = \kappa I(r) e^{-\kappa z}. \tag{9}$$

Substituting Eq. (8) into Eq. (9), we obtain:

$$Q(r,z) = \kappa I_0 \exp\left(-\frac{2r^2}{\omega^2}\right) e^{-\kappa z}. \tag{10}$$

The total absorbed power within the entire lens of thickness d and radius R is determined by integrating the absorbed power density over the entire lens volume, expressed as:

$$P_{\text{abs}} = \int_0^d \int_0^R Q(r,z)\, 2\pi r\, dr\, dz. \tag{11}$$

For weakly absorbing media $\kappa \ll n$ and $R \gg \omega_0$, this formula approximates to:

$$P_{\text{abs}} \approx P_0\left(1 - e^{-\kappa d}\right). \tag{12}$$

This result indicates that, in the case of weak absorption, the absorbed power is linearly proportional to the lens thickness. To optimize power delivery at the target surface, the focal spot size should be minimized to ensure maximum beam concentration at the cutting position.

Table 2. Physical properties of fused silica [13, 14, 27, 28].

Property	**Fused silica**
$\frac{dn}{dT}$ [K^{-1}]	10×10^{-6}
Physical density, ρ [kg/m^3]	2210
Heat capacity, c_p [$J/(kg \cdot K)$]	746
Thermal conductivity, k [$W/(m \cdot K)$]	1.38
Coefficient of thermal expansion [K^{-1}]	0.55×10^{-6}
Initial temperature, T_0 [K]	293.75
Real part of refractive index at T_0	1.45

Therefore, determining focal shift variations and analyzing the influence of thermal lensing on beam quality is a key objective of this study. These aspects will be further discussed in the following sections. The values of the thermophysical parameters of fused silica [13, 14, 27, 28] are presented in Table 2.

3. Results and discussion

3.1. Numerical simulation of thermal lensing effects

Simulation results show that at an average laser power of 6 kW, the lens temperature peaks at 952 K at the center of the collimating lens due to high laser energy density and its greater thickness, while the minimum temperature of the focusing lens ranges from 487 K to 621 K depending on its focal length (125-300 mm), indicating that thermal effects primarily depend on laser power and focal length. Additionally, a detailed analysis reveals that the collimating lens exhibits a larger temperature gradient than the focusing lens, attributed to its greater thickness (10.425 mm compared to 5.321–8.7976 mm, in Table 1.) and proximity to the laser source, resulting in higher thermal accumulation.

The temperature distribution along the x-axis indicates that the collimating lens experiences stronger thermal effects than the focusing lens, with a higher peak temperature (greater presence of lighter shades on the collimating lens in Fig. 2).

As observed in Fig. 3, the temperature distribution approximates a parabolic pattern within a narrow range around the lens center ($x \approx 25$ mm), with the collimating lens reaching a maximum temperature of approximately 952 K at the center, while the focusing lens exhibits a lower peak temperature of around 870 K at its center. The temperature gradually decreases toward the lens edges, reflecting the localized laser energy absorption concentrated at the center.

3.2. Investigation of focal shift

As mentioned earlier, the RMS beam radius represents the focusing capability of the laser beam at the focal plane. Fig. 4 illustrates the dependence of the RMS spot size on the focal position (z) in a laser focusing system using a focusing lens with a focal length of 125 mm, under

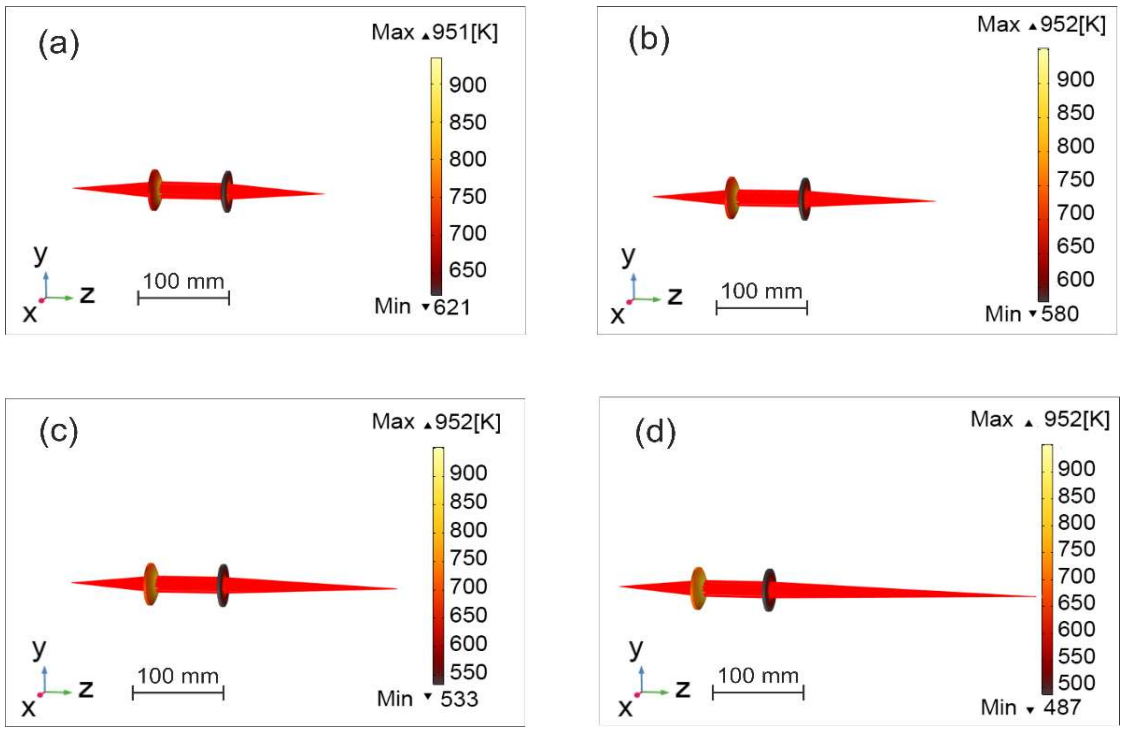

Fig. 2. Temperature distribution and ray tracing with varying focal lengths of the focusing lens 125 mm (a), 150 mm (b), 200 mm (c), and 300 mm (d) at 6 kW average laser power.

varying average laser power levels (P_0) from 1 W (reference) to 6 kW. The RMS spot size curve exhibits a parabolic trend, where the minimum value (parabola vertex) represents the optimal focal position, which shifts progressively toward the lens as the laser power increases from 1 W to 6 kW. Specifically, at $P_0 = 1$ W, the optimal focal position is located at $z = 158.7$ mm, whereas at 6 kW, it shifts to approximately 151.1 mm. The focal shift makes it challenging to maintain optimal focusing without adjusting the focal position, potentially resulting in an overall degradation of beam focusing quality.

Figure 5a illustrates the dependence of focal shift (Δf) on the average laser power (P_0) for focusing lenses with different focal lengths, derived from the parabolic vertex of the RMS spot size function in Fig. 4. The results indicate that Δf increases linearly with increasing average laser power, with a steeper slope for longer focal lengths, reflecting stronger thermal effects in lenses with longer focal lengths. The negative values of Δf indicate that the focal point shifts toward the lens, opposite to the laser beam propagation direction. Specifically, for a focusing lens with $f_2 = 125$ mm, the focal shift is $\Delta f = -7.78$ mm, whereas for $f_2 = 300$ mm, the focal shift reaches $\Delta f = -45.4$ mm at $P_0 = 6$ kW. Longer focal length lenses exhibit larger focal shifts due to a reduced convergence angle, which maintains a larger beam diameter and increases thermal accumulation by extending the interaction area and time within the lens material. Fig. 5b shows the relationship between the maximum temperature (T_{max}) and the deposited power (P_{dep}) on the collimating lens, with both parameters increasing linearly as the average laser power (P_0) rises from 0 to 6 kW. At

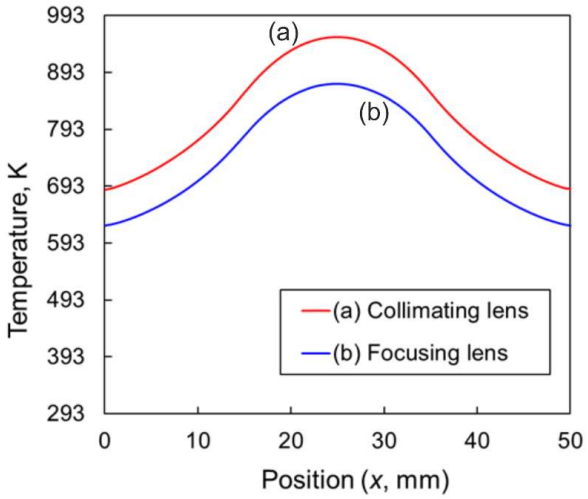

Fig. 3. (Color online) Temperature distribution along the x-axis of collimating and focusing lenses ($f_2 = 125\,\text{mm}$) in a 6 kW laser average power.

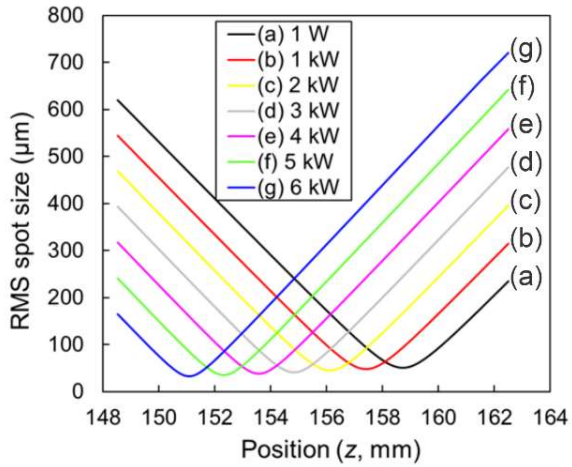

Fig. 4. (Color online) RMS spot size as a function of focal position for a 125 mm converging lens across varying average laser powers.

$P_0 = 1\,\text{W}$, the maximum temperature $T_{\max} = 293.15\,\text{K}$, which corresponds to the initial temperature set in the simulation. At $P_0 = 6\,\text{kW}$, the highest temperature on the collimating lens reaches 952 K, consistent with the results in Fig. 2 and Fig. 3. The linear dependence of focal shift and maximum temperature on laser power (as shown in Fig. 5) aligns well with recent theoretical and experimental studies [13–16]. At $P_0 = 6\,\text{kW}$, the deposited power density on the collimating lens reaches $7.54\,\text{mW}/\text{mm}^3$.

In [16], the authors experimentally investigated the thermal focal shift of a plano-convex lens made of fused silica under a 1 kW laser at a wavelength of 1030 nm. Their results, obtained

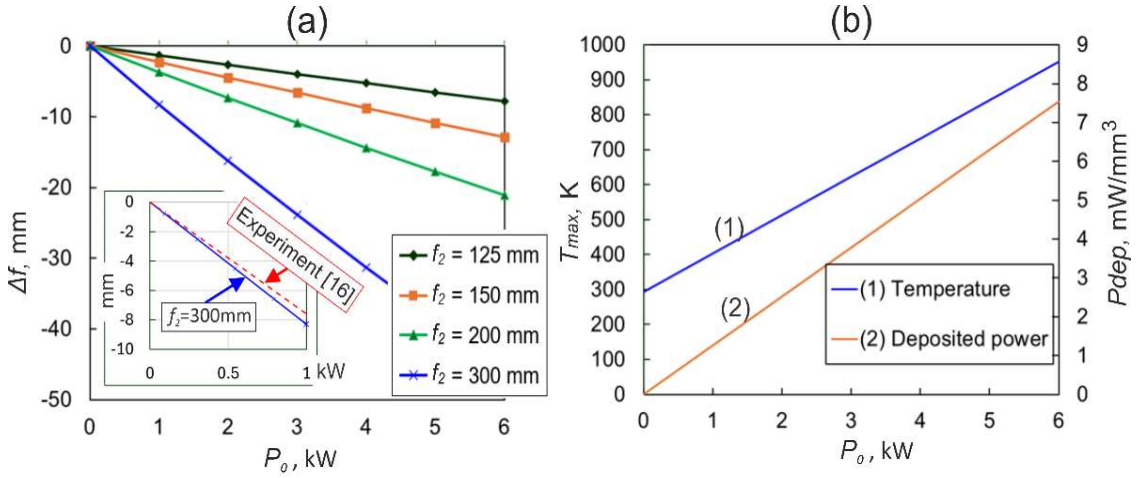

Fig. 5. (Color online) Focal shifts for focusing lenses with varying focal lengths (a) and maximum temperature and deposited power on the collimating lens (b).

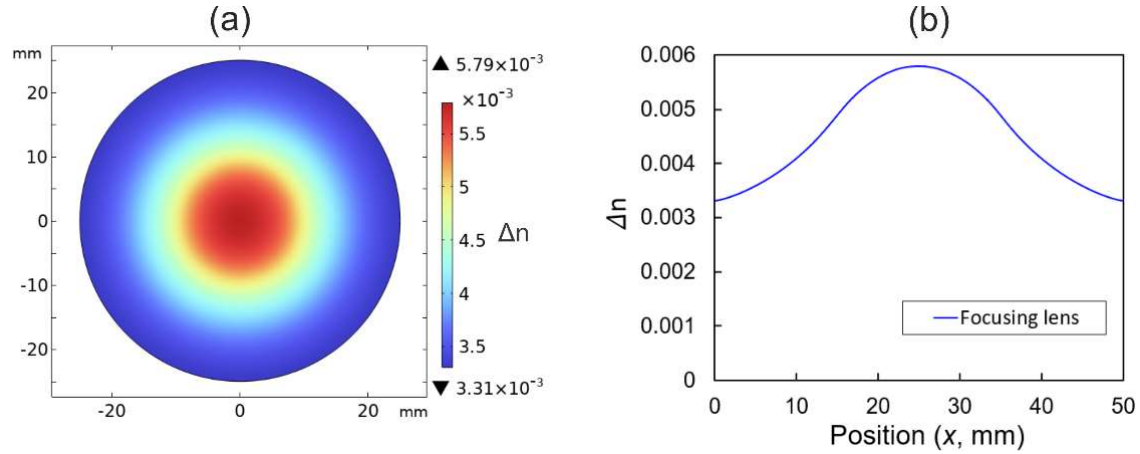

Fig. 6. Spatial (a) and x-axial distribution of refractive index change (b) in a 125 mm focusing lens at 6 kW laser averange power.

with a 300 mm focal length lens coated for that specific wavelength, showed a focal shift exceeded twice the Rayleigh length ($z_R = 3.62$ mm) [16], which is in good agreement with the simulation result in this study: at the same power level (1 kW) and $f_2 = 300$ mm, the focal shift reaches -8.29 mm (see the inset in the lower left corner of Fig. 5a). The spatial variation of the refractive index change (Δn) in the focusing lens with $f_2 = 125$ mm under $P_0 = 6$ kW is depicted in Fig. 6. The maximum value of Δn occurs at the lens center and gradually decreases toward the outer edge. This behavior can be attributed to the Gaussian beam intensity distribution, which results in higher energy density at the center, leading to a strong temperature gradient. Additionally, the lens thickness is greatest at the center, further amplifying the effect. The variation of Δn from

the center to the periphery (Fig. 6b) exhibits a near-parabolic profile, with the maximum value at the lens center and decreasing toward the edges, reflecting the strong temperature gradient at the center (Fig. 3) and explaining why the focal shift (Δf) is negative (Fig. 5a), causing the focal point to move closer to the lens. The larger Δn at the center induces a converging thermal lens effect, enhancing the beam's convergence.

The relative variation between the maximum ($\Delta n_{\max}$) and minimum ($\Delta n_{\min}$) values of the refractive index change is defined as: $\bar{\Delta n} = \dfrac{\Delta n_{\max} - \Delta n_{\min}}{\Delta n_{\min}} \cdot 100\%$. A higher value of $\bar{\Delta n}$ indicates a stronger refractive index change at the lens center compared to its outer edge, which can lead to a greater focal shift, thereby enhancing the thermal lensing effect.

For a focusing lens with $f_2 = 125\,\text{mm}$ at $P_2 = 6\,\text{kW}$ (Fig. 6), $\bar{\Delta n}$ is calculated as 74.5%. Using a similar computational approach, $\bar{\Delta n}$ values were determined for both the collimating lens and the focusing lens across different f_2 values and average laser power levels. These results are summarized in Fig. 7.

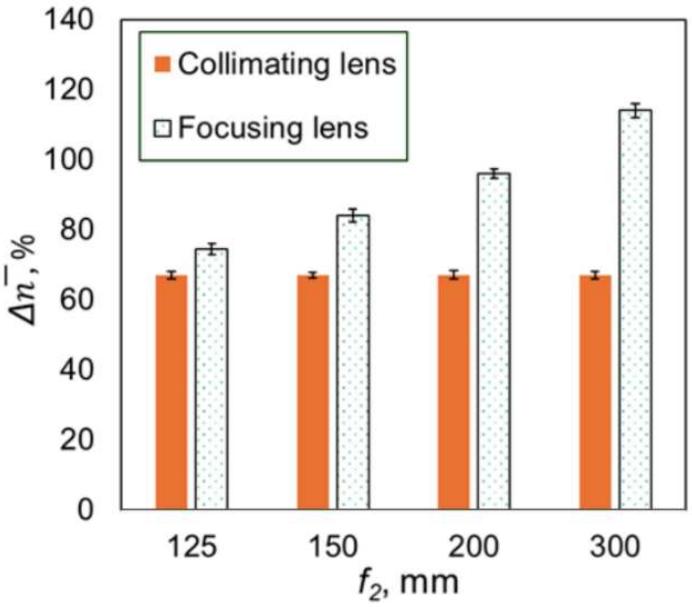

Fig. 7. Relative variation of refractive index change ($\bar{\Delta n}$) between the center and edge of collimating and focusing lenses at different focal lengths (f_2).

Fig. 7 shows the relative variation of the refractive index change ($\bar{\Delta n}$) between the center and edge of the collimating and focusing lenses at different focal lengths (f_2). The relative refractive index variation between the center and the edge of the focusing lens ranges from 74.5% to 114%, corresponding to f_2 values from 125 mm to 300 mm. This increase reflects a larger refractive index gradient in lenses with longer focal lengths, contributing to greater focal shift (see Fig. 5a). The average laser power levels (1–6 kW) introduce minor deviations, on the order of a few percent, for each lens. These uncertainties are represented by error bars on the top of the columns in Fig. 7.

3.3. Numerical artifacts and beam distortion behavior at the focal plane

To evaluate beam quality at the focal plane, we analyze the spot diagram representing the beam distribution. As the refractive index changes with increasing laser power, it acts as an additional virtual thermal lens within the optical system, degrading beam quality. The azimuthal angle (azi, [°]) is defined in the XY-plane at the focal plane as $\arctan(y/x)$, where x and y represent the horizontal and vertical coordinates. The magnitude of azi indicates the angular deviation of rays from the ideal beam center in the focal plane, with a maximum value of 5.74°. Fig. 8 presents the spot diagram at the focal plane for a focusing lens with $f_2 = 125\,\text{mm}$, at average laser power levels of 1 W, 2 kW, 4 kW, and 6 kW. At 1 W – the reference power level (Fig. 8a) – thermal lensing

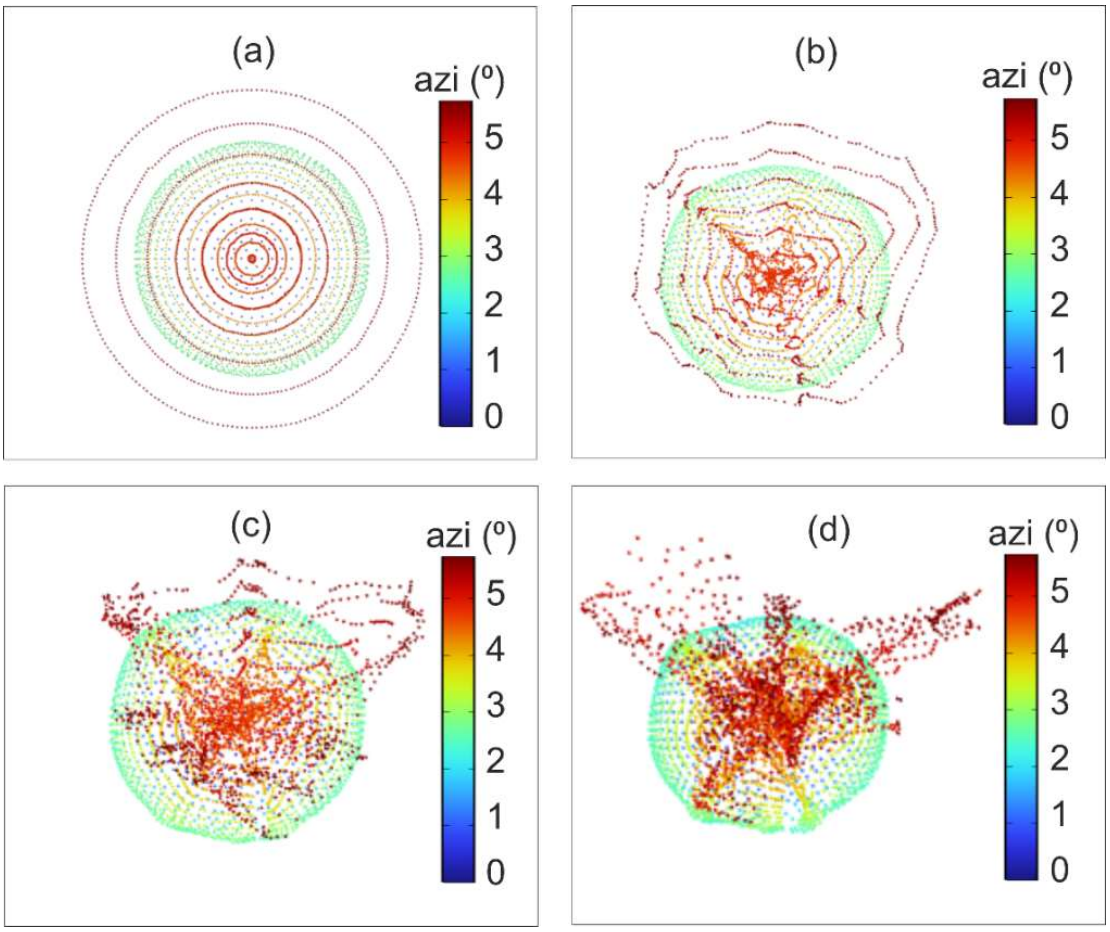

Fig. 8. Spot diagram at the focal plane for a 125 mm focusing lens at varying average laser powers 1 W (a), 2 kW (b), 4 kW (c) and 6 kW (d).

effects are negligible, and the beam remains well-focused due to the low temperature and minimal refractive index changes. This is evident from the uniform and concentric circular spots in the spot diagram. As the laser power increases to 2 kW, beam distortion becomes noticeable, with the

spot diagram exhibiting deformed circular patterns. At higher power levels, the beam deviation intensifies, particularly for rays at larger azimuthal angles. It should be emphasized that the beam distortions shown in Fig. 8 are mainly numerical artifacts of the FEM simulation [29, 30]. The asymmetry is likely caused by the finite number of traced rays and the mesh discretization. Under the present simulation conditions (9000 rays and mesh refinement down to 0.025 mm at the target plane), the FEM approach remains reliable for beam quality analysis up to laser powers of 2 kW. At higher powers, the steep refractive index gradients can amplify numerical errors. Therefore, caution is required when interpreting FEM-predicted distortions, especially if the number of traced rays is insufficient or the mesh is not fine enough.

4. Conclusion

This study presented a numerical investigation of thermal lensing in 1064 nm high-power fiber laser cutting heads (1–6 kW) using two fused silica plano-convex lenses, with focusing lens focal lengths of 125–300 mm. Simulations show a peak lens temperature of 952 K at 6 kW, causing significant focal shifts from $\Delta f = -7.78$ mm (125 mm) to $\Delta f = -45.4$ mm (300 mm) at $P_0 = 6$ kW. The refractive index at the lens center varies 74.5–114% more than at the periphery, depending on power and focal length. Spot diagram analysis shows that beam asymmetry becomes more pronounced at higher laser power levels. This behavior can arise from limitations of the FEM model, particularly when using a finite number of traced rays or a coarse mesh to solve the temperature and refractive index fields, which increases sensitivity to steep refractive index gradients.

Future work may focus on experimental validation through real-time lens temperature measurements, non-contact camera-based sensing of focal shift, and beam quality assessment, as well as improvements in simulation accuracy such as mesh refinement and enhanced ray tracing. In practical laser cutting, mitigating thermal lensing is essential for maintaining beam quality and cutting accuracy. Feasible approaches include active cooling of optical elements, adaptive focusing or optical compensation to correct focal shift, and optimizing lens materials and coatings to reduce absorption. Combined with FEM-based predictions, these strategies can help enhance the stability and performance of high-power fiber laser cutting systems.

Conflict of interest

The author declare no conflicts of interest.

References

[1] K. Kim, M.-K. Song, S.-J. Lee, D. Shin, J. Suh and J.-D. Kim, *Fundamental study on underwater cutting of 50 mm-thick stainless steel plates using a fiber laser for nuclear decommissioning*, Appl. Sci. **12** (2022) 495.

[2] J. S. Shin, S. Y. Oh, H. Park, T.-S. Kim, L. Lee, C.-M. Chung *et al.*, *Underwater cutting of 50 and 60 mm thick stainless steel plates using a 6-kw fiber laser for dismantling nuclear facilities*, Opt. Laser Technol. **115** (2019) 1.

[3] A. Sharma and V. Yadava, *Experimental analysis of nd-yag laser cutting of sheet materials–a review*, Opt. Laser Technol. **98** (2018) 264.

[4] J. S. Shin, K.-H. Song, S. Y. Oh and S.-K. Park, *Laser cutting studies on 10–60 mm thick stainless steels with a short focus head for nuclear decommissioning*, Opt. Laser Technol. **169** (2024) 110121.

[5] A. Sen, B. Doloi and B. Bhattacharyya, *Fiber laser micro-machining of engineering materials*, in *Non-traditional Micromachining Processes*, G. Kibria, B. Bhattacharyya and J. Davim, eds., Springer, (2017).

[6] K. Zhang, S. Xiao, W. Liu, D. Wang and G. Zhang, *Feasibility study of an adjustable-power laser cutting head for tbm applications: focus on rock fragmentation efficiency and energy consumption*, Tunn. Undergr. Space Technol. **155** (2025) 106155.

[7] J. S. Shin, S. Y. Oh, H. Park, C.-M. Chung, S. Seon, T.-S. Kim *et al.*, *High-speed fiber laser cutting of thick stainless steel for dismantling tasks*, Opt. Laser Technol. **94** (2017) 244.

[8] C. Jacinto, D. Messias, A. Andrade, S. Lima, M. Baesso and T. Catunda, *Thermal lens and z-scan measurements: thermal and optical properties of laser glasses–a review*, J. Non-Cryst. Solids **352** (2006) 3582.

[9] A. Gatej and P. Loosen, *Methods for compensation of thermal lensing based on thermo-optical (top) analysis*, Proc. SPIE **9131** (2014) 109.

[10] L. Tatzel and F. P. León, *Impact of the thermally induced focus shift on the quality of a laser cutting edge*, J. Laser Appl. **32** (2020) 022013.

[11] W. M. Steen and J. Mazumder, *Laser Material Processing*. Springer, 2010, 10.1007/978-1-84996-062-5.

[12] K. Dobek, *Thermal lensing: outside of the lasing medium*, Appl. Phys. B **128** (2022) 18.

[13] X. Liu, L. Liu, J. Zhou, L. Sun, Y. Liu and Y. Liang, *Simulated and experimental study on temperature induced lens focal shifts*, Optoelectron. Lett. **15** (2019) 245.

[14] X. Liu, L. Liu, J. Zhou, L. Sun, Y. Liu and Y. Liang, *Study on passive compensation of temperature induced thermal lenses*, Optoelectron. Lett. **16** (2020) 161.

[15] N. Harrop, S. Wolf, O. Maerten, K. Dudek, S. Ballach and R. Kramer, *Absorption driven focus shift*, High-Power Laser Materials Processing: Lasers, Beam Delivery, Diagnostics, and Applications V **9741** (2016) 97410P.

[16] S. Faas, D. J. Foerster, R. Weber and T. Graf, *Determination of the thermally induced focal shift of processing optics for ultrafast lasers with average powers of up to 525 w*, Opt. Express **26** (2018) 26020.

[17] Raytools, "Technical specifications for tube cutting applications." `https://www.raytools.ch/application/3`, 2025.

[18] I. Photonics, "Cutting heads brochure." `https://cdn.ipgphotonics.com/440b783f-8fcf-49bb-8098-b0ec01559c48/IPG_Cutting-Head_BR_EN_LTR.pdf`, 2019.

[19] Osprilaser, "Laser cutting head overview." `https://www.osprilaser.com/laser-cutting-head/`, 2025.

[20] T. Gischkat, D. Schachtler, I. Stevanovic, Z. Balogh-Michels, R. Botha, A. Bächli *et al.*, *Substrate cleaning processes and their influence on the laser resistance of anti-reflective coatings*, Appl. Sci. **10** (2020) 8496.

[21] L. Wan, J. Yang, X. Liu, J. Zhu, G. Xu, C. Hao *et al.*, *Enhanced antireflective and laser damage resistance of refractive-index gradient SiO_2 nanostructured films at 1064 nm*, Polish Journal of Chemical Technology **26** (2024) 0014.

[22] M. H. Maleki, S. Abbasi, M. Vaezzade and A. Asgari, *Improving anti-reflectivity and laser damage threshold of SiO_2/ZrO_2 thin films by laser shock peening at 1064 nm*, Optical and Quantum Electronics **46** (2014) 1149.

[23] E. Safdari, M. Arik, A. M. Basol and M. Budakli, *Micro scale phosphor particles in an led package: Heat transfer, fluid dynamics, optical characteristics*, 23rd IEEE Intersociety Conference on Thermal and Thermomechanical Phenomena in Electronic Systems (ITherm) (2024) 1.

[24] M.-A. Babay, M. Adar, S. Touairi, A. Chebak and M. Mabrouki, *Numerical simulation and thermal analysis of pressurized hydrogen vehicle cylinders: impact of geometry and phase change materials*, J. Adv. Res. Fluid Mech. Therm. Sci. **117** (2024) 71.

[25] D. B. Leviton and B. J. Frey, *Temperature-dependent absolute refractive index measurements of synthetic fused silica*, Proceedings of SPIE **6273** (2006) 62732K.

[26] C. Z. Tan and J. Arndt, *The refractive index of silica glass and its dependence on pressure, temperature, and the wavelength of the incident light*, Silicon-Based Material and Devices (2001) 51.

[27] J. X. Cai, M. Guo and G. Y. Jin, *Numerical simulation of thermal stress damage in 1064 nm anti-reflection fused silica by millisecond pulsed laser*, Optik **136** (2017) 144.

[28] I. H. Malitson, *Interspecimen comparison of the refractive index of fused silica*, J. Opt. Soc. Am. **55** (1965) 1205.

[29] Y. Liu and G. A. Glass, *Effects of mesh density on finite element analysis*, tech. rep., SAE International, Warrendale, PA, USA, 2013. 10.4271/2013-01-1375.

[30] B. A. Rahman and A. Agrawal, *Finite Element Modeling Methods for Photonics*. Artech House, 2013.